Chromophore–Catalyst Assemblies

DOI: 10.1002/anie.201305951

Low-Overpotential Water Oxidation by a Surface-Bound Ruthenium-Chromophore–Ruthenium-Catalyst Assembly**

*Michael R. Norris, Javier J. Concepcion, Zhen Fang, Joseph L. Templeton, and Thomas J. Meyer**

Producing solar fuels by artificial photosynthesis requires the integration of light absorption with electron/proton transfer events to drive both water oxidation and reduction of protons to hydrogen or of CO_2 to carbon fuels.[1–5] One approach is the use of molecular assemblies in dye-sensitized photoelectrosynthesis cells (DSPECs). In photoanode applications, they combine light absorption and catalysis in single molecular assemblies. Chromophore excitation and electron injection into the conduction band of a large band gap semiconductor, typically TiO_2, are followed by rapid electron-transfer activation of a linked molecular catalyst.[6–10] Progression through a series of excitation/electron transfer reactions provides the necessary oxidative equivalents for overall, light-driven water oxidation.[11]

Molecular assemblies are attractive candidates for DSPEC applications owing to their versatility and variability based on synthetic modifications. We have reported on the electrochemical and photophysical properties of a family of Ru-based chromophore–catalyst assemblies, both in solution,[12–14] and bound to metal-oxide surfaces, such as ZrO_2, TiO_2, and nanostructured tin-doped indium oxide, nano-ITO.[14,15] As illustrated in Equation (1) on TiO_2, excitation of

$$\begin{aligned} TiO_2\text{–}[Ru_a^{II}\text{–}Ru_b^{II}\text{–}OH_2]^{4+} &\xrightarrow{h\nu} TiO_2\text{–}[Ru_a^{II*}\text{–}Ru_b^{II}\text{–}OH_2]^{4+} \\ &\rightarrow TiO_2(e^-)\text{–}[Ru_a^{III}\text{–}Ru_b^{II}\text{–}OH_2]^{5+} \\ &\rightarrow TiO_2(e^-)\text{–}[Ru_a^{II}\text{–}Ru_b^{III}\text{–}OH_2]^{5+} \end{aligned} \quad (1)$$

the surface-bound chromophore is followed by excited state electron injection and intra-assembly electron transfer, which initiate oxidative activation of the catalyst.

From studies on single-site ruthenium–polypyridyl catalysts, water oxidation occurs mechanistically by stepwise proton-coupled electron transfer (PCET) oxidation of Ru^{II}–OH_2^{2+} to $Ru^{IV}{=}O^{2+}$. Further $1e^-$ oxidation to $Ru^{V}(O)^{3+}$ triggers water oxidation.[14,16–18] Examples of single-site and assembly catalysts are shown in Figure 1 with [Ru(tpy)-(Mebim-py)$(OH_2)]^{2+}$ (**1**, tpy = 2,2′:6′,2″-terpyridine; Mebim-py = 2-pyridyl-*N*-methylbenzimidazole)[16] and [$(bpy)_2$Ru(4-Mebpy-4′-bimpy)Ru(tpy)$(OH_2)]^{4+}$ (**2**, bpy = 2,2′-bipyridine; 4-Mebpy-4′-bimpy = 4-(methylbipyridin-4′-yl)-*N*-(benzimid)-*N*′-pyridine); tpy = 2,2′:6′,2″-terpyridine).[13]

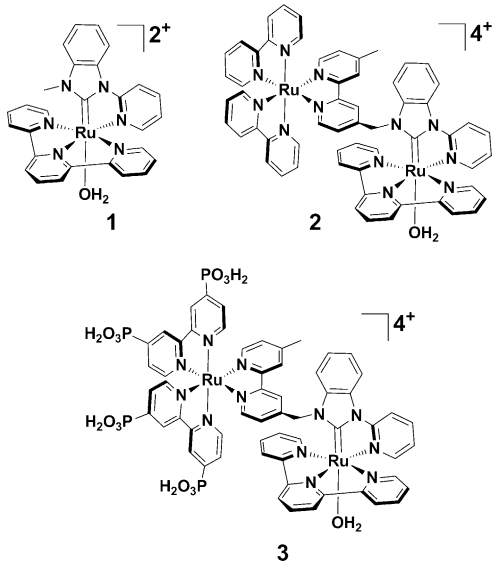

Figure 1. Structures of single-site catalyst **1**,[16] solution-based assembly **2**, and the phosphonic acid-derivatized chromophore-catalyst assembly **3**.

The multi-electron/multi-proton nature of oxidative activation poses a challenge for DSPEC schemes based on single-photon, single-electron events. Given the $3e^-/2H^+$ requirement for catalyst activation in **2**, an isolated assembly must absorb and use three photons with the sequence of events in Equation (1) followed by two additional excitation–injection–electron-transfer cycles in competition with back electron transfer [Eq. (2)].

$$TiO_2(e^-)\text{–}[Ru_a^{II}\text{–}Ru_b^{III}\text{–}OH_2]^{5+} \xrightarrow{-e^-} TiO_2\text{–}[Ru_a^{II}\text{–}Ru_b^{II}\text{–}OH_2]^{4+} \quad (2)$$

Equation (1) also establishes energy requirements for water oxidation. In assembly **2**, the formal potential for the chromophore couple is $E^{\circ\prime}$ ($Ru_a^{III/II}$) 1.36 V vs. NHE. At pH 1, $E^{\circ\prime}$ values for the $[Ru_a^{II}\text{–}Ru_b^{IV}{=}O]^{4+}/[Ru_a^{II}\text{–}Ru_b^{III}\text{–}OH_2]^{5+}$ and $[Ru_a^{II}\text{–}Ru_b^{III}\text{–}OH_2]^{5+}/[Ru_a^{II}\text{–}Ru_b^{II}\text{–}OH_2]^{4+}$ couples are 1.15 and 0.90 V, respectively. $E^{\circ\prime}$ for the pH-independent $[-Ru_b^{V}(O)]^{3+}/[-Ru_b^{IV}{=}O]^{2+}$ couple is about 1.55 V, 0.19 V above the potential for oxidation of the chromophore [Ru_a^{III}–

[*] M. R. Norris, Dr. J. J. Concepcion, Dr. Z. Fang, Prof. J. L. Templeton, Prof. T. J. Meyer
Department of Chemistry
University of North Carolina at Chapel Hill
CB#3290 Chapel Hill, NC 27599-3290 (USA)
E-mail: tjmeyer@unc.edu

[**] This work was wholly funded by the UNC Energy Frontier Research Center (EFRC) "Center for Solar Fuels", an EFRC funded by the U.S. Department of Energy, Office of Science, Office of Basic Energy Sciences, under Award DE-SC0001011.

Supporting information for this article is available on the WWW under http://dx.doi.org/10.1002/anie.201305951.

$]^{3+}/[Ru_a^{II}–]^{2+}$ couple. Based on these values, the final step in a $3e^-/2H^+$ light-driven, oxidative activation to give $TiO_2(e^-)–[Ru_a^{III}–Ru_b^{IV}=O]^{5+}$ would leave the surface-bound assembly 200 mV short of reaching the active $[–Ru_b^{V}(O)]^{3+}$ form of the catalyst. This could create a kinetic roadblock to photochemical water oxidation.

A solution to this dilemma was suggested in a previous kinetic study on water oxidation by **2** with Ce^{IV} as the oxidant in acidic solution.[13] These experiments revealed a redox "mediator" effect for the assembly with a rate enhancement of about 8 compared to single-site catalyst **1**. The effect was attributed to equilibrium population of the unfavorable redox isomer, $[Ru_a^{II}–Ru_b^{V}(O)]^{5+}$, followed by rate-limiting Ce(IV) oxidation to $[Ru_a^{III}–Ru_b^{V}(O)]^{6+}$, and rapid water oxidation (Scheme 1).

$$[Ru_a^{III}\text{-}Ru_b^{IV}=O]^{5+} \rightleftharpoons [Ru_a^{II}\text{-}Ru_b^{V}(O)]^{5+} : K$$

$$Ce^{IV} + [Ru_a^{II}\text{-}Ru_b^{V}(O)]^{5+} \rightarrow Ce^{III} + [Ru_a^{III}\text{-}Ru_b^{V}(O)]^{6+} : k$$

$$[Ru_a^{III}\text{-}Ru_b^{V}(O)]^{6+} + 2H_2O + Ce^{IV} \rightarrow [Ru_a^{III}\text{-}Ru_b^{II}\text{-}OH_2]^{4+} + Ce^{III} + O_2 + 2H^+ : \text{rapid}$$

Scheme 1. Proposed origin of the redox mediator effect in Ce^{IV}-driven water oxidation by **2**.

The synthesis of **3** was achieved in a stepwise, one-pot method (see the Supporting Information for experimental details). Hydrolyzed product precipitated from the reaction mixture in good yield and high purity (for ^1H and ^{31}P NMR, see the Supporting Information, Figures S1, S2), with HPLC analysis of crude **3** showing only a small amount of unreacted chromophore (Supporting Information, Figure S3), which was removed by column chromatography. Only the isomer with the solvent molecule *trans* to the carbene (Figure 1) is observed, consistent with **1** and **2**.[13,16]

Cyclic voltammetry measurements (CVs) on **3** were carried out on glass slides coated with fluoride-doped tin oxide (FTO) by immersing the slide in a 0.1 mM solution of **3** in 0.1M HNO_3 for 20 min. The loaded slide was used as the working electrode with a Ag/AgCl (3M NaCl) reference (0.207 V vs. NHE) and a platinum mesh counter electrode in buffered aqueous solutions. A CV of **3** (Figure 2) in 0.1M $HClO_4$ shows a similar oxidation pattern as for **2**. In positive scans, a reversible oxidation wave is observed at 0.90 V vs. NHE for the $FTO–[Ru_a^{II}–Ru_b^{III}–OH_2]^{5+}/FTO–[Ru_a^{II}–Ru_b^{II}–OH_2]^{4+}$ couple followed by a second oxidation for the $FTO–[Ru_a^{II}–Ru_b^{IV}=O]^{4+}/[FTO–Ru_a^{II}–Ru_b^{III}–OH_2]^{5+}$ couple at 1.15 V.

As found for related couples,[19] the wave for the $FTO–[Ru_a^{II}–Ru_b^{IV}=O]^{4+}/FTO–[Ru_a^{II}–Ru_b^{III}–OH_2]^{5+}$ couple is distorted from kinetic effects arising from the loss of two protons in solutions more acidic than $pH = pK_a \approx 4.5$ for $[Ru_a^{II}–Ru_b^{III}–OH_2]^{3+}$. A reversible $FTO–[Ru_a^{III}–Ru_b^{IV}=O]^{5+}/FTO–[Ru_a^{II}–Ru_b^{IV}=O]^{4+}$ wave appears at 1.36 V. This oxidation triggers water oxidation, and the oxidation of $FTO–[Ru_a^{III}–Ru_b^{IV}=O]^{5+}$ to $FTO–[Ru_a^{III}–Ru_b^{V}(O)]^{6+}$ at about 1.5 V is lost in the catalytic current.

As expected, the $Ru^{III/II}$ and $Ru^{IV/III}$ couples for the catalyst in **3** are pH-dependent, although there are surface-

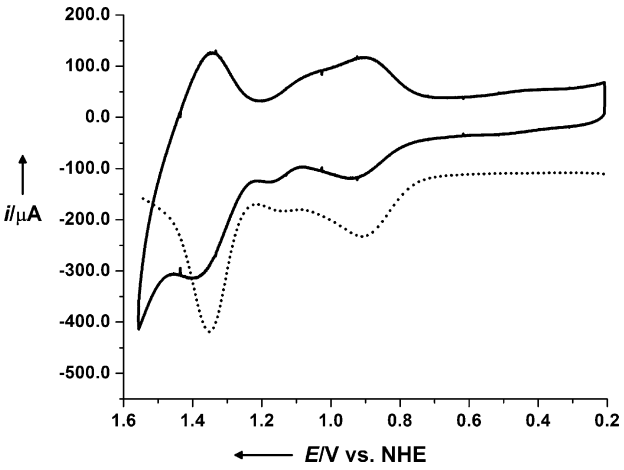

Figure 2. Cyclic voltammogram (solid, 10 $mV s^{-1}$) and square wave voltammogram (dashed) of **3** attached to FTO in 0.1 M $HClO_4$ with a Ag/AgCl reference (3 M NaCl, 0.207 V vs. NHE) and Pt mesh counter electrode at 298 ± 3 K.

induced deviations from Nernstian behavior. From the results in the Supporting Information, Figure S4, and similar to results on related Ru catalysts[16,20] and Ru catalyst–chromophore assemblies at low pH,[12,13,15] from pH 1–3 the $FTO–[Ru_a^{II}–Ru_b^{III}–OH_2]^{5+}/FTO–[Ru_a^{II}–Ru_b^{II}–OH_2]^{4+}$ couple is pH independent while the potential for the $FTO–[Ru_a^{II}–Ru_b^{IV}=O]^{4+}/FTO–[Ru_a^{II}–Ru_b^{III}–OH_2]^{5+}$ couple decreases by 130 mV/pH unit consistent with a $1e^-/2H^+$ couple. Above pH 3, the $FTO–[Ru_a^{II}–Ru_b^{III}–OH_2]^{5+}/FTO–[Ru_a^{II}–Ru_b^{II}–OH_2]^{4+}$ and $FTO–[Ru_a^{II}–Ru_b^{IV}=O]^{4+}/FTO–[Ru_a^{II}–Ru_b^{III}–OH_2]^{5+}$ couples overlap and become indistinguishable. The potential for these couples decreases by 35 mV/pH unit rather than by 59 mV/pH unit as expected for the $2e^-/2H^+$ couple $FTO–[Ru_a^{II}–Ru_b^{IV}=O]^{4+}/FTO–[Ru_a^{II}–Ru_b^{II}–OH_2]^{4+}$. Similar effects have been observed for related surface-bound assemblies and attributed to interfacial electric field effects.[15] As observed in a related assembly,[15] oxidation of the chromophore in **3** is also slightly pH dependent with $E^{o\prime}$ decreasing by about 20 mV/pH unit.

Water oxidation was investigated by rotating ring-disk electrode (RRDE) voltammetry. In these experiments, **3** was attached to a film of mesoporous, nano-structured, tin-doped indium oxide (nanoITO) on the glassy carbon disk of the RRDE, as described in the Supporting Informationand as previously reported.[21] The assembly was anchored to the surface by immersion in a 0.1 mM solution of **3** in 0.1M HNO_3 (Figure 3).

CVs of the resulting surface-bound couple, $nanoITO–[Ru_a^{II}–Ru_b^{III}–OH_2]^{5+}/nanoITO–[Ru_a^{II}–Ru_b^{II}–OH_2]^{4+}$ (Supporting Information, Figure S5) were used to determine the surface loading of **3** by use of Equation (3) and integrating the

$$\Gamma = \frac{Q}{AFn} \tag{3}$$

area under the wave form. In Equation (3), Q is the charge passed (by integration with correction for the scan rate), A is the area of the electrode in cm^2, F is Faraday's constant, and n is the number of electrons transferred. From the CV in the

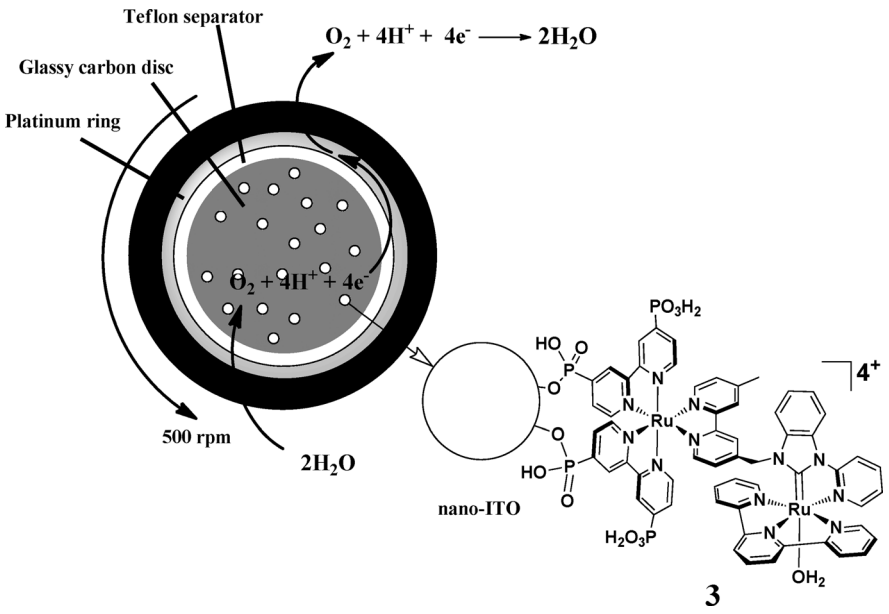

Figure 3. Diagram of the modified RRDE derivatized with nanoITO and loaded with **3**. Oxygen produced at the modified disk is detected at the ring.

Supporting Information, Figure S5, the surface coverage of **3** was found to be 5.5×10^{-9} mol cm^{-2}.

Oxygen measurements were carried out at the Pt ring of the RRDE at a rotation rate of 500 rpm by dual-electrode cyclic voltammetry (DECV). The disk was scanned from 0.9 V to 1.62 V at a scan rate of 10 mV s^{-1} to electrochemically oxidize **3**. The potential of the ring was held at −0.017 V to detect oxygen, which is rapidly reduced to water under these conditions (Supporting Information, Figure S6).[21]

The collection efficiency at the ring depends on the geometry of the electrode which, for the electrode used, was found to be 25 %.[21] With scans to positive potentials, the disk current of **3** on nanoITO shows an increase at about 1.2 V for the nanoITO–$[Ru_a^{II}–Ru_b^{III}–OH_2]^{5+}$/nanoITO–$[Ru_a^{II}–Ru_b^{II}–OH_2]^{4+}$ couple. It is followed by a large increase in current beginning at about 1.3 V for the closely spaced oxidations of nanoITO–$[Ru_a^{II}–Ru_b^{III}–OH_2]^{5+}$ to nanoITO–$[Ru_a^{II}–Ru_b^{IV}=O]^{4+}$ and nanoITO–$[Ru_a^{II}–Ru_b^{IV}=O]^{4+}$ to nanoITO–$[Ru_a^{III}–Ru_b^{IV}=O]^{5+}$. Scanning past 1.30 V resulted in further increases in the disk current, which reached a maximum at about 1.55 V. The ring current over the same potential range mirrors the current produced at the disk, confirming the appearance of O_2 generated electrocatalytically at the disk. In this configuration, the water oxidation onset potential occurs at 1.40 V, an overpotential of 230 mV relative to 1.17 V for the O_2/H_2O couple at pH 1. The ring current continues to increase, tracking the disk current, until oxidation to nanoITO–$[Ru_a^{III}–Ru_b^{IV}=O]^{5+}$ at about 1.55 V. It then decreases slightly as the disk current decreases (Supporting Information, Figure S6).

The Faradaic efficiency for water oxidation was calculated from the fraction of disk current leading to oxygen reduction at the ring (Supporting Information, Figure S7). As expected, the oxygen collection efficiency mirrors the *i–V* curve in the DECV experiment. The current-to-oxygen efficiency reaches a maximum of about 28 % at 1.53 V and begins to diminish as the applied potential is increased further. The less than 100 % Faradaic O_2 yield is currently under investigation and appears to be due in part to oxidation of the exposed glassy carbon surface at the disk and to partial catalyst decomposition.[21]

The turnover frequency (TOF) of **3** as a function of potential was also determined based on the surface coverage of 5.5×10^{-9} mol cm^{-2} (Figure 4). TOFs were calculated based on the ring current by use of Equation (4). In

$$\mathrm{TOF} = \frac{i}{nF\Gamma A} \qquad (4)$$

Equation (4), i is the current in A, n is the number of electrons transferred, F is Faraday's constant, Γ is the surface coverage in mol cm^{-2}, and A is the area of the electrode in cm^2. It is important to note that the TOF calculated from the ring current is a direct measurement of O_2 production and takes into account the Faradaic efficiency of the system.

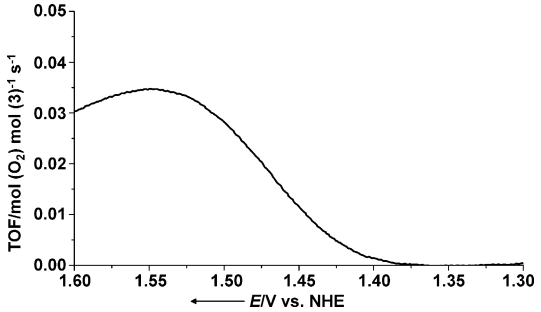

Figure 4. Turnover frequency (TOF in mol O_2 per mol **3** per second) versus applied potential for electrocatalytic water oxidation by **3** on nanoITO on the disk of a modified RRDE. TOFs were evaluated from the current outputs in DECV experiments from the ring current. The values cited are lower limits owing to loss of **3** from the surface during water oxidation. Electrochemical evaluation of surface coverage is complicated following water oxidation owing to the appearance of peroxide intermediates on the surface.[18,20,23,24]

For single-site catalyst **1**, water oxidation is triggered by oxidation of $Ru^{IV}=O^{2+}$ to $Ru^{V}(O)^{3+}$ at about 1.55 V. Based on the DECV results on nanoITO–$[Ru_a^{II}–Ru_b^{III}–OH_2]^{5+}$, the onset for water oxidation at pH 1 begins at 1.40 V, which coincides with the potential for oxidation of the surface-bound chromophore, nanoITO–$[Ru_a^{II}–Ru_b^{IV}=O]^{4+} \xrightarrow{-e^-}$ nanoITO–$[Ru_a^{III}–Ru_b^{IV}=O]^{5+}$ (Figure 2, $E_{1/2}$ = 1.36 V). The potential is significantly lower than the potential required for direct oxidation of the catalyst to $Ru^{V}(O)^{3+}$ (1.55 V), and the overpotential (230 mV) is one of the lowest reported for water oxidation at pH 1. A related observation has been reported for a single-site $Ru^{IV}=O$

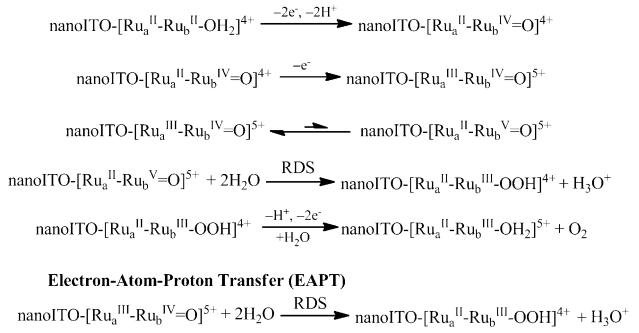

Scheme 2. Proposed mechanism(s) for water oxidation by **3** on nanoITO.

catalyst by Fujita and co-workers. They proposed that the extra oxidative equivalent was provided by an electrode or chemical oxidant in concert with water attack.[22]

A proposed mechanism for water oxidation catalysis by assembly **3** is shown in Scheme 2. It follows from the results of the electrochemical studies and meets the requirement for $3e^-/2H^+$ oxidative activation followed by rate limiting water attack on the oxo group. Based on the results of earlier mechanistic and theoretical studies, reaction with water occurs by O-atom transfer in concert with proton transfer to a second water molecule or water cluster in a reaction described as Atom-Proton Transfer (APT).[17,20]

The ability of the assembly to oxidize water with a relatively low overpotential, while avoiding prior oxidation to $Ru^V(O)^{3+}$, is a significant finding. As implied by the mechanism in Scheme 2, the key may lie in use of the high energy redox isomer, nanoITO–[Ru_a^{II}–Ru_b^{V}=O]$^{5+}$ or, as suggested by Fujita and co-workers,[22] concerted electron–atom–proton transfer (EAPT). In this reaction, O-atom transfer occurs from $-Ru^{IV}$=O to a water molecule with simultaneous proton release occurring in concert with intra-assembly electron transfer to $-Ru_a^{III}-$.[19] In either case, the results show $3e^-/2H^+$ activation of water oxidation at potentials achievable with light for this system.

Although rates of water oxidation by the assembly are relatively slow with TOF = 0.04 s^{-1}/O_2 produced, as measured by the oxygen current at the ring, significant rate enhancement occurs with added buffer bases owing to the intervention of concerted atom–proton transfer pathways.[19] Rate enhancements through APT pathways and solar water splitting on TiO_2 by this assembly are currently under investigation.

Received: July 9, 2013
Revised: October 9, 2013
Published online: November 7, 2013

Keywords: chromophore–catalyst assemblies · electrocatalysis · rotating ring-disk electrodes · ruthenium · water oxidation

[1] N. S. Lewis, D. G. Nocera, *Proc. Natl. Acad. Sci. USA* **2006**, *103*, 15729.
[2] D. G. Nocera, *ChemSusChem* **2009**, *2*, 387.
[3] J. J. Concepcion, J. W. Jurss, M. K. Brennaman, P. G. Hoertz, A. O. v. T. Patrocinio, N. Y. Murakami Iha, J. L. Templeton, T. J. Meyer, *Acc. Chem. Res.* **2009**, *42*, 1954.
[4] R. Eisenberg, H. B. Gray, *Inorg. Chem.* **2008**, *47*, 1697.
[5] M. R. Wasielewski, *Acc. Chem. Res.* **2009**, *42*, 1910.
[6] W. Song, C. R. K. Glasson, H. Luo, K. Hanson, M. K. Brennaman, J. J. Concepcion, T. J. Meyer, *J. Phys. Chem. Lett.* **2011**, *2*, 1808.
[7] J. A. Treadway, J. A. Moss, T. J. Meyer, *Inorg. Chem.* **1999**, *38*, 4386.
[8] H. Gerischer, *Electrochim. Acta* **1993**, *38*, 3.
[9] H. Gerischer, *Electrochim. Acta* **1995**, *40*, 1277.
[10] Y. Xu, G. Eilers, M. Borgström, J. Pan, M. Abrahamsson, A. Magnuson, R. Lomoth, J. Bergquist, T. Polívka, L. Sun, V. Sundström, S. Styring, L. Hammarström, B. Åkermark, *Chem. Eur. J.* **2005**, *11*, 7305.
[11] W. J. Youngblood, S.-H. A. Lee, K. Maeda, T. E. Mallouk, *Acc. Chem. Res.* **2009**, *42*, 1966.
[12] D. L. Ashford, D. J. Stewart, C. R. Glasson, R. A. Binstead, D. P. Harrison, M. R. Norris, J. J. Concepcion, Z. Fang, J. L. Templeton, T. J. Meyer, *Inorg. Chem.* **2012**, *51*, 6428.
[13] M. R. Norris, J. J. Concepcion, D. P. Harrison, R. A. Binstead, D. L. Ashford, Z. Fang, J. L. Templeton, T. J. Meyer, *J. Am. Chem. Soc.* **2013**, *135*, 2080.
[14] J. J. Concepcion, J. W. Jurss, P. G. Hoertz, T. J. Meyer, *Angew. Chem.* **2009**, *121*, 9637; *Angew. Chem. Int. Ed.* **2009**, *48*, 9473.
[15] D. L. Ashford, W. Song, J. J. Concepcion, C. R. K. Glasson, M. K. Brennaman, M. R. Norris, Z. Fang, J. L. Templeton, T. J. Meyer, *J. Am. Chem. Soc.* **2012**, *134*, 19189.
[16] J. J. Concepcion, J. W. Jurss, M. R. Norris, Z. Chen, J. L. Templeton, T. J. Meyer, *Inorg. Chem.* **2010**, *49*, 1277.
[17] Z. Chen, J. J. Concepcion, X. Hu, W. Yang, P. G. Hoertz, T. J. Meyer, *Proc. Natl. Acad. Sci. USA* **2010**, *107*, 7225.
[18] J. J. Concepcion, J. W. Jurss, J. L. Templeton, T. J. Meyer, *J. Am. Chem. Soc.* **2008**, *130*, 16462.
[19] Z. Chen, A. K. Vannucci, J. J. Concepcion, J. W. Jurss, T. J. Meyer, *Proc. Natl. Acad. Sci. USA* **2011**, *108*, E1461.
[20] J. J. Concepcion, M.-K. Tsai, J. T. Muckerman, T. J. Meyer, *J. Am. Chem. Soc.* **2010**, *132*, 1545.
[21] J. J. Concepcion, R. A. Binstead, L. Alibabaei, T. J. Meyer, *Inorg. Chem.* **2013**, *52*, 10744.
[22] D. E. Polyansky, J. T. Muckerman, J. Rochford, R. Zong, R. P. Thummel, E. Fujita, *J. Am. Chem. Soc.* **2011**, *133*, 14649.
[23] Z. Chen, J. J. Concepcion, J. F. Hull, P. G. Hoertz, T. J. Meyer, *Dalton Trans.* **2010**, *39*, 6950.
[24] A. K. Vannucci, J. F. Hull, Z. Chen, R. A. Binstead, J. J. Concepcion, T. J. Meyer, *J. Am. Chem. Soc.* **2012**, *134*, 3972.

